A Modified STRUCT Model for Efficient Engineering Computations of Turbulent Flows with Rotation and Curvature

Chaoyue Wang[1], Fujun Wang[1]*, Chenfeng Li[2], Changliang Ye[1], Tingting Yan[1], Zhichao Zou[3]

[1]*College of Water Resources and Civil Engineering, China Agricultural University, Beijing, 100083, China*

[2]*College of Engineering, Swansea University, Swansea, SA1 8EN, United Kingdom*

[3]*China Institute of Water Resources and Hydropower Research, Beijing, 100038, China*

Abstract: A modified STRUCT turbulence model (MST model) for efficient engineering computations of turbulent flows with rotation and curvature is proposed in this paper. The MST model switches between URANS and LES-like modes using a new damping function to adjust the turbulent viscosity. Compared with the original STRUCT method, the modifications are as follows: (1) the BSL k-ω model with the Spalart-Shur correction is chosen as the new baseline to improve the sensitivity to rotation and curvature; (2) a new adaptive time-scale ratio is proposed to avoid the arbitrariness of geometric averaging operation in the original method; (3) the normalized helicity is introduced into the new damping function to detect the energy backscatter phenomenon. Five classical high Reynolds number flow cases are tested. The results show that the turbulent viscosity of flow in the massively separated regions modeled by the MST model is reasonably reduced, and LES-like mode is activated, which captures more turbulent vortices and fluctuations on the URANS grids. With high efficiency and robustness, the MST model inherits the advantages of the original STRUCT method and improves the prediction accuracy of turbulent flows with rotation and curvature, which enables efficient engineering computations of the turbulence in hydraulic rotating machinery.

Keywords: STRUCT, turbulence model, rotation and curvature, hydraulic rotating machinery

*Corresponding Author.
E-mail Address: wangfj@cau.edu.cn (Fujun Wang).

HIGHLIGHTS

A modified STRUCT turbulence model, MST model, is proposed.

A new URANS baseline is used to improve the sensitivity to rotation and curvature.

A new time-scale ratio is used to improve the adaptability of damping function to flow fields.

The normalized helicity is introduced to detect the energy backscatter phenomenon.

A good accuracy-cost balance is achieved for simulation of hydraulic rotating machinery.

1 Introduction

Hydraulic rotating machineries, such as pumps and hydroturbines, play an important role in the energy industry, and their energy conversion characteristics are determined by the inner flows, whose Reynolds number is typically 10^5~10^6 during operation. The inner turbulent flows in hydraulic rotating machineries are strongly affected by the rotation and curvature effects, and they are one of the most complicated flow cases in engineering. Two basic turbulence models, URANS (Unsteady Reynolds-averaged Navier-Stokes) and LES (Large Eddy Simulation), have been commonly used to simulate the inner turbulent flows in hydraulic rotating machineries [1]. The URANS method is based on the Reynolds averaging in the statistical sense of the instantaneous Navier-Stokes equations, the accuracy of which remarkably depends on the analysist's experience and the choice of boundary conditions, and it is usually difficult to obtain high-precision prediction results of complex separation flows [2]. The LES approach is based on the spectral filtering of turbulence energy, and in great detail it captures the large eddies that carry most of the turbulent kinetic energy and are responsible for most of the momentum transportation and turbulence mixing [3]. LES is generally more accurate than URANS, but the high computational cost has hampered its practical application [4]. For a better tradeoff of prediction accuracy and computational cost, some hybrid approaches have been proposed, such as hybrid URANS/LES and the second generation URANS (2G-URANS) approaches.

The hybrid URANS/LES approach has been a popular topic in recent years. A transition from URANS to LES can be achieved in two ways [5-6]. One strategy is to use a weighted sum of the Reynolds stress from the URANS model and the subgrid-scale stress from the LES model (*blending*), and the other strategy is to use a pure LES model in one part of the domain and a pure URANS model in the remainder (*interfacing*). The detached eddy simulation (DES) method is one of the most popular hybrid URANS/LES approaches [7]. The original DES model switches from the URANS mode in the boundary layer to the LES mode in the main flow, and the switching criterion is based on the grid size and the wall distance. In order to solve the problems of "modeled stress depletion" and "log layer mismatch" of the original DES model, the DDES (add the full name here) and IDDES (add the full name here) models are proposed [8-9]. Although the above DES models have been successfully used for the simulation of separation flows, there are some major limitations of these models in engineering applications. First, the priori selection of the desired resolution level and the compatible meshing scheme are required, which is often difficult, if not impossible, for large-scale engineering applications. Secondly, the LES-like local grid refinement is required in the main flow, which consumes a lot of computation resources.

Aiming at resolving the substantial turbulent structures, such 2G-URANS models as VLES (add the full name here) [10-12], PANS (add the full name here) [13-15], SAS (add the full name here) [16-18] and FBM (add the full name here) [19-20] models, have emerged, and they do are not explicitly dependent on the computation grid like the DES models. The VLES model can be obtained by rescaling a conventional URANS model through damping the Reynolds stress with a function that controls the ratio of modeled energy to resolved energy. The PANS model is based on the self-similarity scale assumption in the physical space, and a seamless transition from URANS to DNS (direct numerical simulation) can be realized by using a damping function to adjust the given URANS model. The SAS model introduces the Von Kármán length scale and is able to switch from the URANS mode to the SAS mode where the related physical length scale is reduced yielding a lower turbulent viscosity and high fluctuations. The FBM model introduces the ratio of a

turbulence length scale to a filter size and aims to obtain a lower turbulent viscosity. Although the aforementioned 2G-URANS models do not explicitly depend on the computation grid, the grid space scale is still needed to calculate the damping function, which may cause requirements on grid conditions and affect the simulation efficiency and robustness.

Different from the above hybrid approaches that bridge URANS and LES using the space scale of grids, the STRUCT (add full name here) method [22-23] uses the turbulent timescale to determine the damping function and it maintains the efficiency and robustness of URANS while extending the ability to locally resolve complex turbulent vortices. A variety of flow cases have demonstrated the LES-like capability of STRUCT on coarse grids, with a significant reduction of computation time. In addition, a consistent accuracy improvement can be achieved by increasing the mesh resolution [22,24]. These features make the STRUCT method an attractive approach for efficient computation of turbulent flows in hydraulic rotating machineries.

However, the original STRUCT method is not without limitation. Firstly, the turbulent flows in hydraulic rotating machineries are strongly affected by the rotation and curvature effects, which may result in a remarkable energy backscatter phenomenon [25]. The original STRUCT method does not consider the energy backscatter appropriately, which may cause local over-dissipation and give unreasonable results. Secondly, as a key activation parameter of the original STRUCT method, the modeled timescale can be determined by means of the geometric averaging operation or the additional convective-diffusive transport equation [22-23]. The former is more suitable for efficient engineering computations, but it may lead to an unsuitable value due to the arbitrary identification threshold of flow structures. Thirdly, the damping function in the near wall region always goes to 1, where the ordinary URANS mode is employed. As the base URANS model of the original STRUCT method, the standard k-ε model is not an ideal choice. To address these limitations, this paper presents a modified STRUCT model (*MST*), and five classical flow cases with high Reynolds number are employed to test the performance of the new model, including the turbulent swirling flow through an abrupt axisymmetric expansion, flow around a hydrofoil, flow past a cylinder, Taylor-Couette flow and flow in a centrifugal pump impeller. For comparison, the classical SST (add full name here) k-ω model is also applied to these test cases.

2 Mathematical Formulation

2.1 The OST model

The original STRUCT method (*OST*) switches between URANS and hybrid modes by using a timescale-based damping function to adjust the turbulent viscosity. The standard k-ε model is used for the baseline URANS, and the transport equations of turbulent kinetic energy k and dissipation rate ε are expressed as [23]

$$\begin{cases} \rho\dfrac{\partial k}{\partial t}+\rho\overline{u}_j\dfrac{\partial k}{\partial x_j}=\dfrac{\partial}{\partial x_j}\left[\left(\mu+\dfrac{\mu_t}{\sigma_k}\right)\dfrac{\partial k}{\partial x_j}\right]+G_k-\rho\varepsilon \\ \rho\dfrac{\partial \varepsilon}{\partial t}+\rho\overline{u}_j\dfrac{\partial \varepsilon}{\partial x_j}=\dfrac{\partial}{\partial x_j}\left[\left(\mu+\dfrac{\mu_t}{\sigma_\varepsilon}\right)\dfrac{\partial \varepsilon}{\partial x_j}\right]+C_{\varepsilon 1}\dfrac{\varepsilon}{k}G_k-C_{\varepsilon 2}\rho\dfrac{\varepsilon^2}{k} \end{cases} \tag{1}$$

where $\overline{u}_j$ is average velocity components, ρ is the water density, t is time coordinates, x_j is spatial coordinates, μ is dynamic viscosity, μ_t is turbulent viscosity, σ_k is the Prandtl number of turbulent

kinetic energy, G_k is the production term of turbulent kinetic energy, σ_ε is the Prandtl number of turbulent dissipation rate, and $C_{\varepsilon 1}$ and $C_{\varepsilon 2}$ are closure constants.

Following the hybrid approach [26], the turbulent viscosity of the OST model is directly adjusted by a damping function D_f:

$$\begin{cases} \mu_t = D_f \cdot \rho C_\mu \dfrac{k_m^2}{\varepsilon} \\ D_f = min\left(\dfrac{t_r}{at_m}, 1\right) \end{cases} \tag{2}$$

where k_m is the modeled turbulent kinetic energy, t_r is the resolved timescale, t_m is the modeled timescale, and C_μ and a are empirical constants. The damping function D_f can also be interpreted as the ratio of modeled turbulent kinetic energy to the total amount of turbulent kinetic energy, and the hybrid mode of OST model is activated when the resolved timescale is lower. In particular, the definitions of the two timescales are expressed as

$$\begin{cases} t_r = \dfrac{1}{f_r} = \dfrac{1}{\sqrt{|Q|}} \\ t_m = \dfrac{1}{f_m} = \left\langle \dfrac{k_m}{\varepsilon} \right\rangle \end{cases} \tag{3}$$

where f_r is the frequency of t_r, f_m is the frequency of t_m, $\langle\cdot\rangle$ represents a generic averaging operation in the concerned region to estimate the modeled timescale, and Q is the second invariant of the resolved velocity gradient tensor given by

$$Q = \frac{1}{2}\left(\|\boldsymbol{\Omega}\|_F^2 - \|\boldsymbol{D}\|_F^2\right) = -\frac{1}{2}\frac{\partial \overline{u_i}}{\partial x_j}\frac{\partial \overline{u_j}}{\partial x_i} \tag{4}$$

where $\|\boldsymbol{\Omega}\|_F$ is the Frobenius norm of rotation rate tensor, and $\|\boldsymbol{D}\|_F$ is the Frobenius norm of strain rate tensor. Due to the outstanding advantages, Galilean invariance and local description in elementary motions, this parameter is suitable for describing properties of the resolved flow field. Fig. 1 shows an illustrative comparison between the STRUCT strategy and other turbulence approaches. The STRUCT method models less scales than LES, thus achieving lower grid requirements and computation cost. Meanwhile, its turbulence capturing ability is greater than URANS, thus obtaining higher simulation accuracy and more turbulent structures.

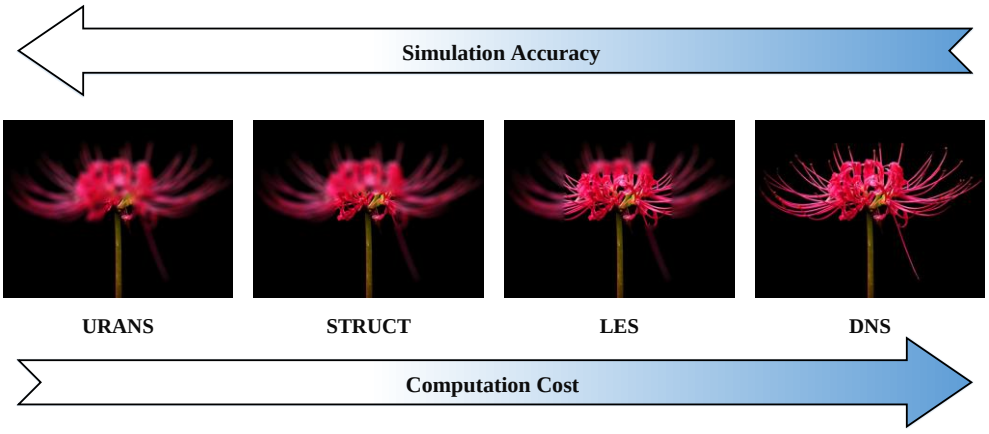

Figure 1. Illustration of STRUCT and other turbulence modelling strategies

2.2 The MST model

We propose the MST model to overcome the limitations of the OST model discussed in Section 1, and the detailed derivation is explained in this section.

- **Baseline Model**

In order to improve the sensitivity to adverse pressure gradients in the turbulent flows with rotation and curvature, the BSL *k-ω* model with the Spalart-Shur correction is employed as the new baseline URANS model. This maintains the robust and accurate formulation of the standard *k-ω* model in the near wall region and takes advantage of the freestream independence of the standard *k-ε* model in the main flow region [27-28]. The transport equations of turbulent kinetic energy *k* and specific dissipation rate *ω* of the BSL *k-ω* model are expressed as [27]

$$\begin{cases} \rho\dfrac{\partial k}{\partial t}+\rho\overline{u}_j\dfrac{\partial k}{\partial x_j}=\dfrac{\partial}{\partial x_j}\left[\left(\mu+\dfrac{\mu_t}{\sigma_{k3}}\right)\dfrac{\partial k}{\partial x_j}\right]+G_k-\beta'\rho k\omega \\ \rho\dfrac{\partial \omega}{\partial t}+\rho\overline{u}_j\dfrac{\partial \omega}{\partial x_j}=\dfrac{\partial}{\partial x_j}\left[\left(\mu+\dfrac{\mu_t}{\sigma_{\omega 3}}\right)\dfrac{\partial \omega}{\partial x_j}\right]+2\rho\left(1-F_1\right)\dfrac{1}{\sigma_{\omega 2}\omega}\dfrac{\partial k}{\partial x_j}\dfrac{\partial \omega}{\partial x_j}+\alpha_3\dfrac{\omega}{k}G_k-\beta_3\rho\omega^2 \end{cases} \tag{5}$$

where $\overline{u}_j$ is average velocity components, ρ is the water density, t is time coordinates, x_j is spatial coordinates, μ is dynamic viscosity, μ_t is turbulent viscosity, G_k is the production term of turbulent kinetic energy, F_1 is a weighted function, and σ_{k3}, $\sigma_{\omega 2}$, $\sigma_{\omega 3}$, α_3, β_3 and β' are closure parameters.

- **Adaptive Time-scale Ratio**

In order to determine an adaptive (automatic and dynamic) modeled timescale t_m, the specific dissipation rate ω with the dimension of "frequency" is directly used in this research. It is obtained from the transport equations and avoids the arbitrariness of the geometric averaging operation and the cost of additional convective-diffusive transport equation [22-23]. Accordingly, the modeled-to-resolved timescale ratio R_t is given by

$$R_t=\frac{t_m}{t_r}=\frac{1}{\varphi\omega}\cdot\sqrt{|Q|} \tag{6}$$

where φ is an empirical constant, whose value is set to 0.085 in this study. The turbulent flows in hydraulic rotating machineries are generally incompressible, and the second invariant Q is still employed to determine the resolved timescale t_r.

- **Consideration of Turbulence Energy Backscatter**

In order to take the energy backscatter phenomenon into account, the *helicity*, a topological measure of the intertwining of vortices and an invariant even in the viscous fluid [29-30], is introduced. The turbulent viscosity diminishing is found to be connected with the limitations of the energy transfer from the larger scales to smaller scales in the presence of helicity [31]. The regions of high helicity fluctuations are found to be closely correlated with the regions of low energy flux owing to the reduction of nonlinear interactions [32]. Moreover, the energy backscatter is stronger than the forward dissipation when the value of normalized helicity H_n exceeds 0.7, and a modified Spalart-Allmaras model with consideration of the energy backscatter is obtained by using the

normalized helicity, which can improve the simulation accuracy of the corner separation flows in the compressor [25]. The normalized helicity H_n is also employed:

$$H_n = \frac{\boldsymbol{V}\cdot(\nabla\times\boldsymbol{V})}{|\boldsymbol{V}|\cdot|\nabla\times\boldsymbol{V}|} = cos[\boldsymbol{V},\nabla\times\boldsymbol{V}] \tag{7}$$

where $\boldsymbol{V}$ is velocity vector, $\nabla\times\boldsymbol{V}$ is the vorticity vector, and $[\cdot]$ represents the vector angle operation. The new damping function of the MST model is redefined as

$$\begin{cases} \mu_t = D_f \cdot \rho \dfrac{k_m}{\omega} \\ D_f = \dfrac{1}{ln\left[ch\left(\alpha\cdot R_t\right)+\beta\right]+\gamma\cdot|H_n|^{\lambda}} \end{cases} \tag{8}$$

where empirical constants, α=1.571, β=1.718, γ=0.727, λ=0.865, are optimized to these values based on the relevant references [22,25], and they are suitable for solving the flow fields with water medium.

In summary, the new D_f of the MST model not only overcomes the limitations of OST but it also activates smoothly, thereby avoiding the step problem caused by the piecewise function of the OST model. The theoretical formulation of MST makes it a more suitable simulation approach for turbulent flows with rotation and curvature.

3 Applications of the MST Model

Five classical flow cases are employed to test the performance of the proposed MST model, and the include turbulent swirling flow through an abrupt axisymmetric expansion, flow around a hydrofoil, flow past a cylinder, Taylor-Couette flow and flow in a centrifugal pump impeller.

3.1 Swirling flow through an abrupt axisymmetric expansion

Turbulent swirling flow through an abrupt axisymmetric expansion is a complex flow case possessing lots of dynamic phenomena such as vortex breakdown, detachment and reattachment, which is similar to the vortex rope in the draft tube of hydroturbine. The computation domain of the abrupt expansion is shown in Fig. 2, corresponding to the experiment [33]. For this flow case, the Reynolds number based on the inlet diameter D and the bulk velocity is approximately 3×10^4, and the swirl number is approximately 0.6.

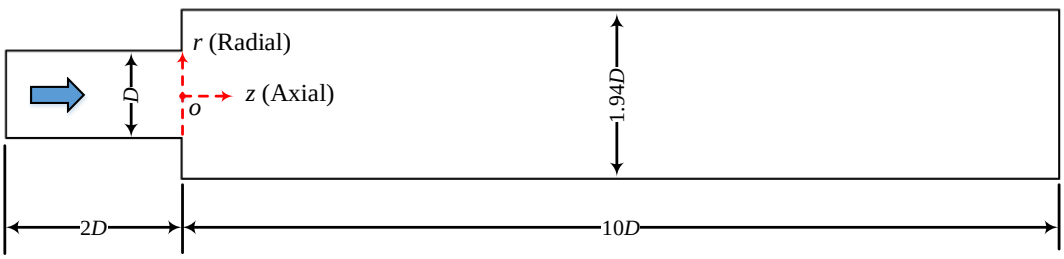

Figure 2. Computation domain and local coordinate frame of the abrupt expansion

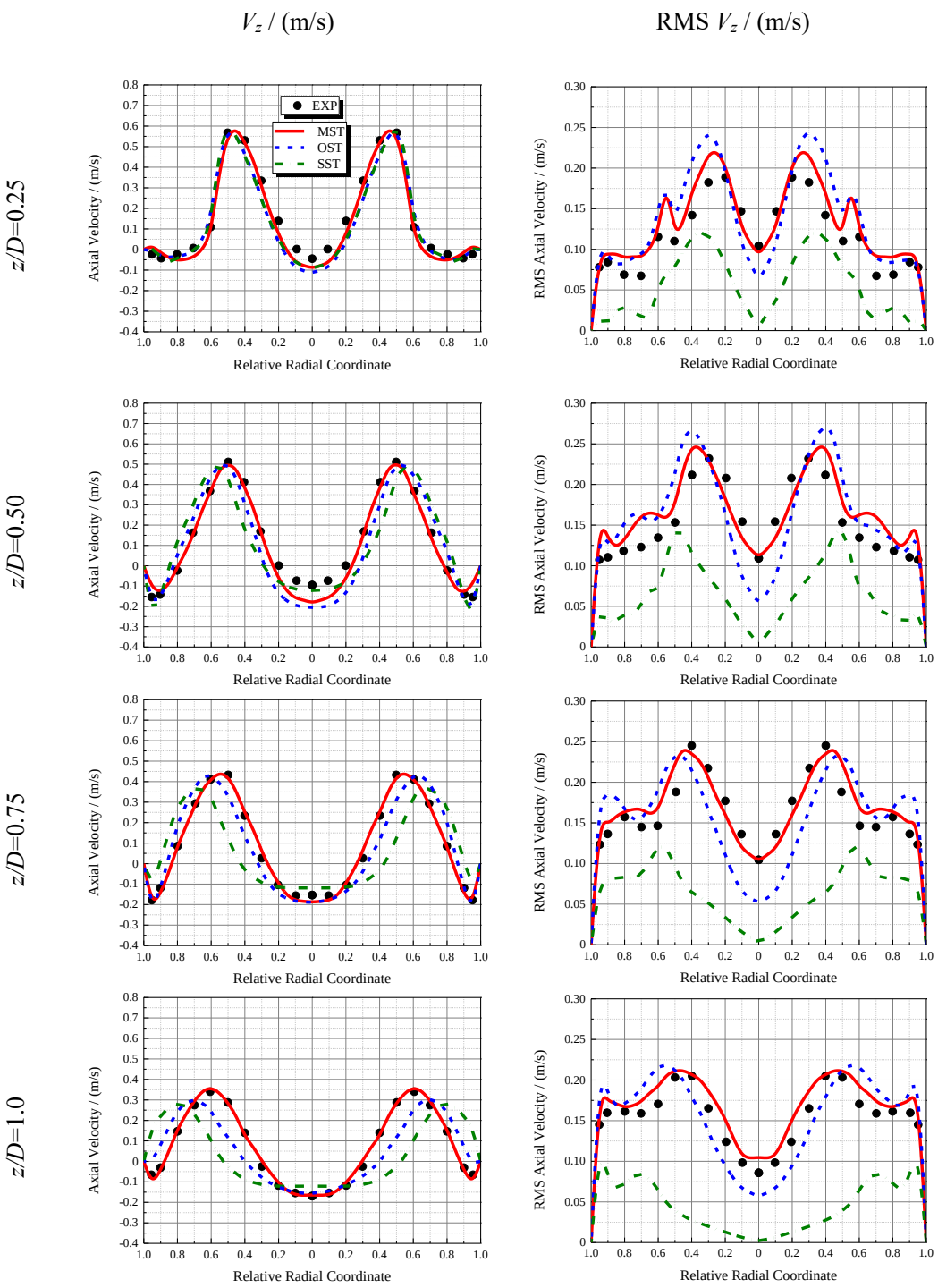

Figure 3. Mean and RMS values of axial velocity

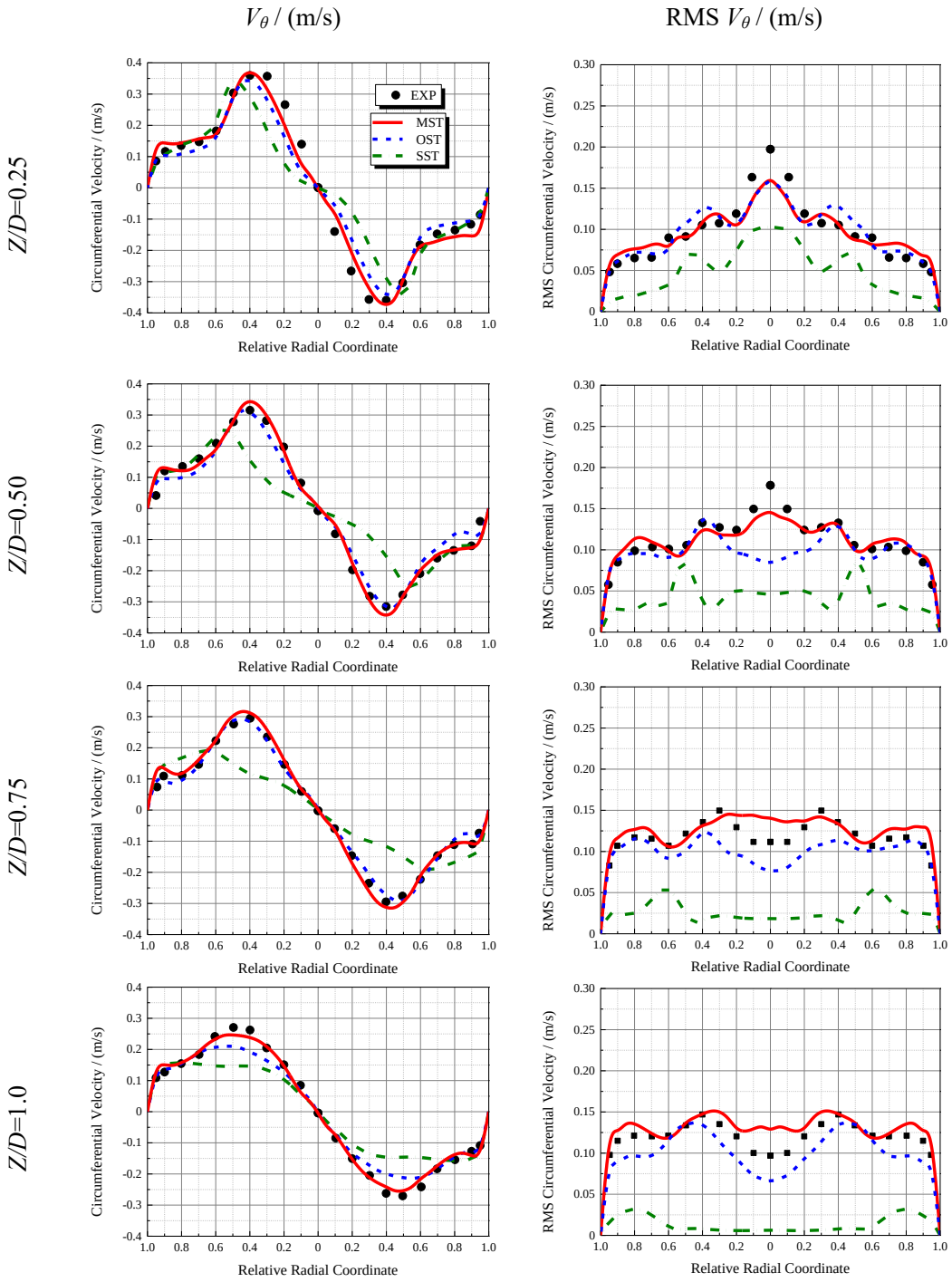

Figure 4. Mean and RMS values of circumferential velocity

As for the meshing scheme, high quality hexahedral grids are adopted to discretize the domain. The discretization mesh is consistent with those used in literatures for this flow case [14,34-35]. In terms of boundary conditions, the velocity inlet condition is used according to the radial profiles obtained from experiment data, and a high inlet turbulence intensity (10%) is also estimated. The pressure outlet condition is adopted, and the no-slip condition is employed for wall surfaces. The key parameter t_m of the OST model is set to 0.5s. Transient simulation is carried out, and the time step is selected to meet the CFL condition. The computation time is not less than 25 times the through-flow period (the period required by the mean flow to pass through the total domain once), and the results below are obtained by using the time-weighted average of the last 12 periods.

Fig. 3 and Fig. 4 show the distributions of the mean and RMS values of axial velocity V_z and circumferential velocity V_θ on four cross sections behind the expansion, corresponding to the z/D values of 0.25~1.0. The results of the MST model are compared with the experiment data as well as those of the OST model and SST k-ω model. It is observed that the SST k-ω model gives poor results of mean and RMS velocity profiles, and especially it captures little turbulent fluctuation information, which implies that the prediction results of this model converge to a steady simulation. The accuracy of OST model is better, but some deviations still exist near the pipe center (r=0), which indicates that the original STRUCT method is insufficient to simulate turbulent flows with rotation and curvature. By contrast, the simulation results of MST model are in good agreement with the experimental data. Moreover, the power spectrum density (PSD) of the MST model is shown in Fig. 5. The resolved scales are asymptotic to an inertial subrange, reasonably close to the classical −5/3 scaling, which implies that the LES-like mode is activated efficiently and the expected improvements are achieved on the basis of the original STRUCT method.

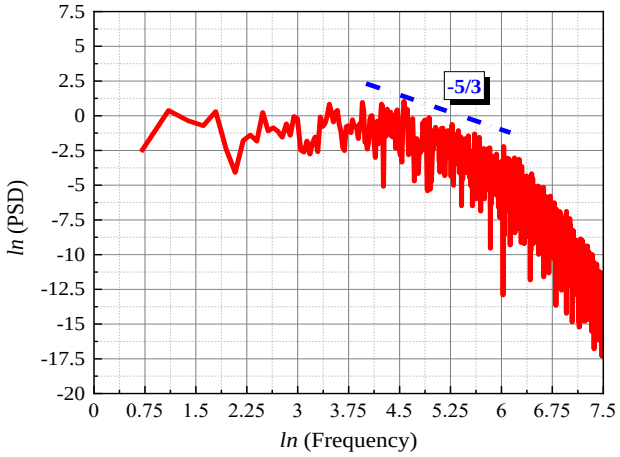

Figure 5. PSD analysis of the MST model

According to the previous researches, the phenomenon, "*a precessing vortex core rotates around the geometrical axis and subsequently breaks down to small coherent structures*", is remarkable. As shown in Fig. 6, the vortical structures are visualized by the isosurfaces of *Liutex* criterion [36]. The SST k-ω model captures a large scale vortex rope, which cannot simulate self-induced unsteady motions of the "vortex breakdown" and results in the above poor results. Both the OST model and the MST model capture the "vortex breakdown", and the latter captures more detailed vortical structures.

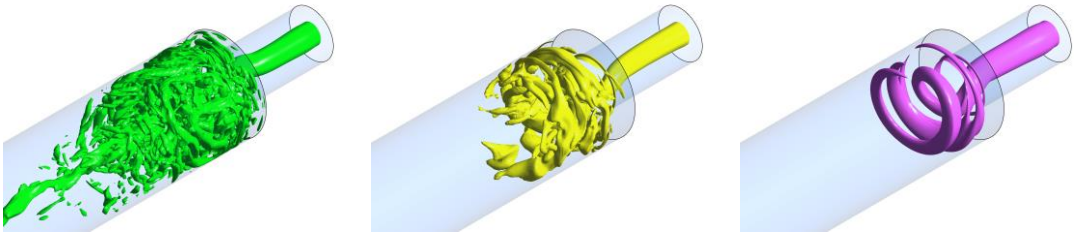

(a) MST (b) OST (c) SST

Figure 6. Vortical structures visualized by isosurfaces of *Liutex* criterion (*Liutex*=30s^{-1})

The average turbulent viscosity ratio and damping function on the plane of z/D=1.0 are shown in Table 1. Compared with the OST model, the damping function of the MST model is reasonably reduced, which effectively adjusts the turbulent viscosity and helps to capture more turbulent

information. The switch between URANS and LES-like modes is more efficient for the MST model, thereby allowing more turbulent vortices and fluctuations to be captured on the same grids.

Table 1. Comparison of the average turbulent viscosity ratio and damping function

z/D=1.0	Viscosity Ratio $\overline{\mu_t / \mu}$	Damping Function $\overline{D_f}$
MST	2.83	0.4
OST	52.72	0.1
SST	177.39	1.0

3.2 Flow around a hydrofoil

Flow around a hydrofoil is a classical case possessing many dynamic phenomena such as flow transition and vortex shedding, which is of great significance to analyze the flow field in the impeller and guide-vane domains in hydraulic rotating machineries. The computation domain of a NACA0009 hydrofoil is shown in Fig. 7, corresponding to the experiment [37]. For this flow case, the Reynolds number based on the chord length L and the free-stream velocity is approximately 2×10^6. A 2D flow obstacle made up of glue and sand combination is placed near the leading edge, which is designated as the "*tripped transition*" in the experiment [38].

As for the meshing scheme, high quality hexahedral grids are adopted to discretize the domain. The discretization mesh is consistent with those reported in literatures [39-40]. In terms of boundary conditions, the velocity inlet condition is used according to the chord Reynolds number, and a medium inlet turbulence intensity (5%) is also estimated. The pressure outlet condition is adopted, and no-slip condition is employed for wall surfaces. The symmetry boundary is also used to reduce the computation cost. The key parameter t_m of the OST model is set to 0.001s. Transient simulation is carried out, and the time step is selected to meet the CFL condition. The computation time is not less than 6 times the through-flow period (the period required by the mean flow to pass through the total domain once), and the results below are obtained by using the time-weighted average of the last 3 periods. Moreover, the classical γ-Reθt transition model is activated for the SST and MST model, both of which are based on the *k-ω* model and ready to be combined with the transition model in engineering computations.

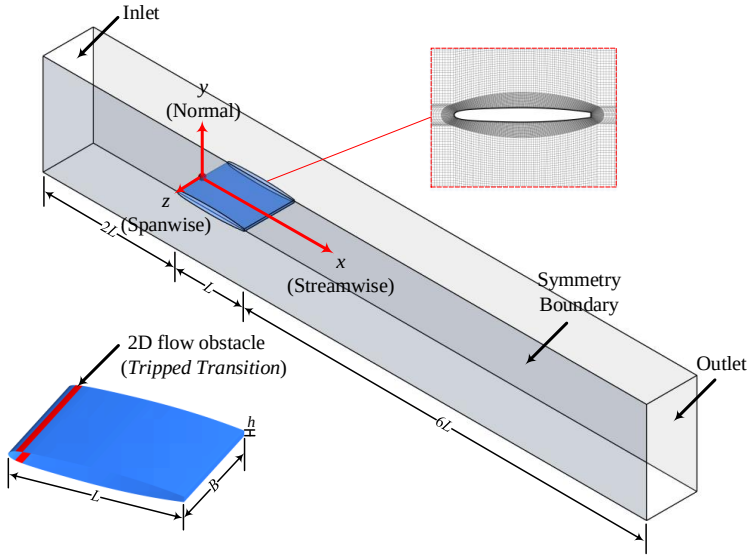

Figure 7. Computation domain and local coordinate frame of the hydrofoil

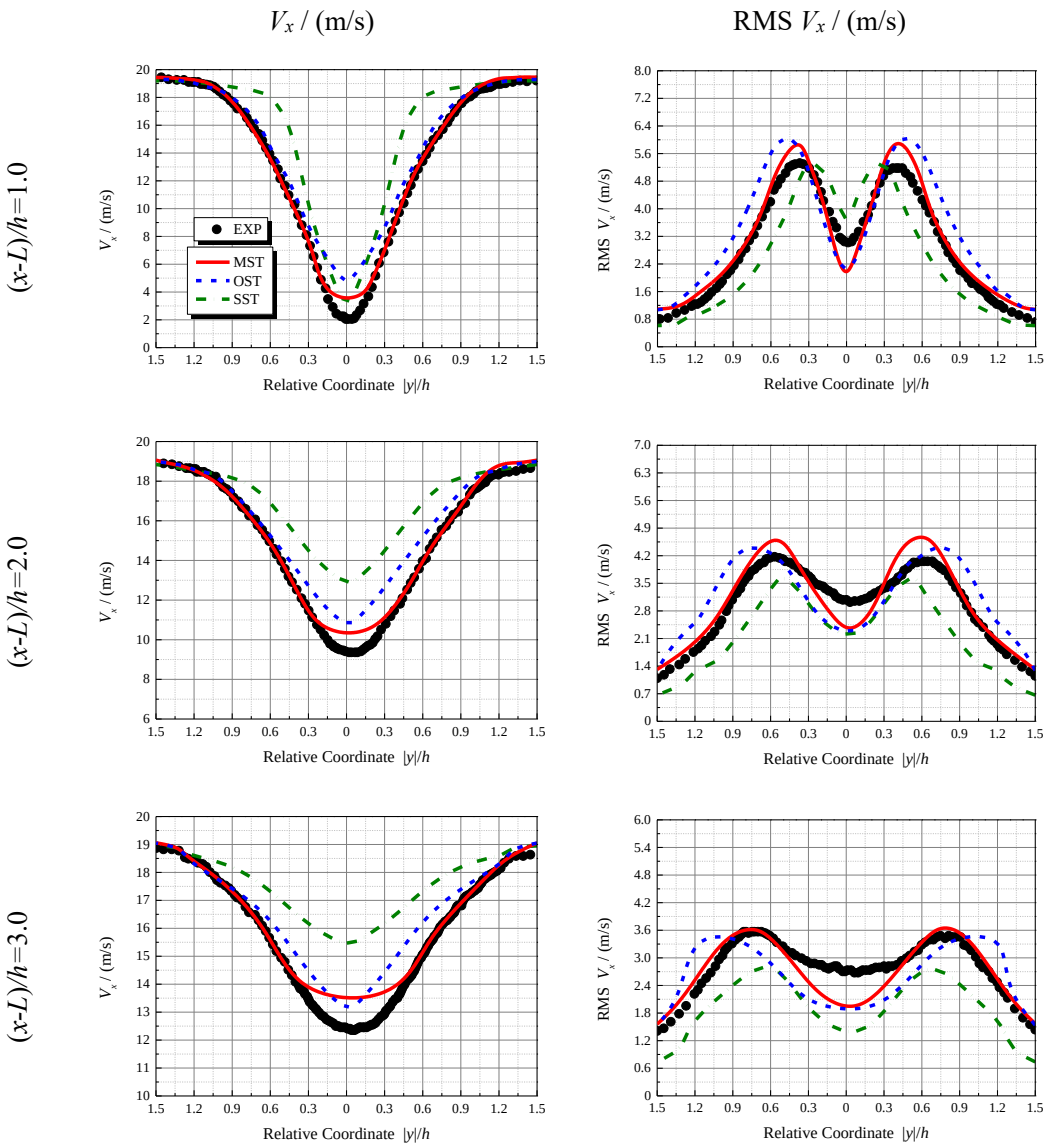

Figure 8. Mean and RMS values of streamwise velocity

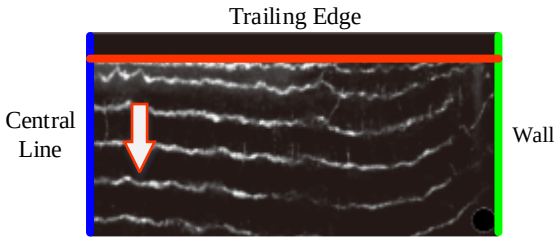

(a) EXP

(b) MST (c) OST (d) SST

Figure 9. Vortex street visualized by *Liutex* isosurfaces (*Liutex*=600s^{-1})

The distributions of the mean and RMS values of streamwise velocity V_x on three measured lines in the *xoy* plane, corresponding to the (*x*-*L*)/*h* values of 1.0~3.0, are shown in Fig. 8. The SST *k*-*ω* model gives poor results of mean and RMS velocity profiles, and little turbulent fluctuation information is captured. The OST model gives better results, but some deviations still exist in the predictions of RMS velocity profiles. By contrast, the accuracy of the MST model is significantly improved. In addition, a comparison of the vortex shedding frequency is shown in Table 2. The relative errors of vortex shedding frequency obtained by the MST and OST models are within 2%, while the value obtained by the SST model is much higher than that of the experiment.

As shown in Fig. 9, the vortical structures are visualized by the isosurfaces of *Liutex* criterion. According to the experiment observation, "*the vortices essentially exhibit a parallel vortex shedding mode for the tripped transition*" [37]. The features of Karman vortex street obtained by MST model are closer to the experimental image. It proves again that the expected improvements by MST.

Table 2. Comparison of the vortex shedding frequency

	Vortex shedding frequency / (Hz)	Relative error
EXP	1078	-
MST	1058.16	1.84%
OST	1092.14	1.31%
SST	1354.62	25.66%

3.3 Flow past a cylinder

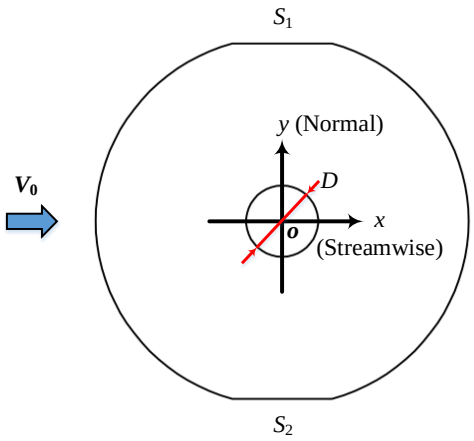

Figure 10. Computation domain and local coordinate frame of the circular cylinder

Flow past a cylinder is also a classical case possessing many important phenomena and has been intensively investigated [41-43]. In this study, the computation domain of a circular cylinder is shown in Fig. 10, corresponding to the experiment [41]. For this flow case, the Reynolds number

based on the diameter D and the free-stream velocity is approximately 1.4×10^5.

High quality hexahedral grids are adopted to discretize the domain, and the discretization mesh is consistent with those reported in literatures [42,44]. The spanwise extension is chosen to be $z=D$. As for boundary conditions, the velocity inlet condition is used according to the Reynolds number, and a low inlet turbulence intensity (1%) is also estimated. The pressure outlet condition is adopted, and the no-slip condition is employed for the wall surfaces. Two symmetry boundary conditions are applied far away from the cylinder (S_1 & S_2), and the translational periodicity condition is employed in the spanwise direction. The key parameter t_m of the OST model is set to 0.001s. Transient simulation is carried out, and the time step is selected to meet the CFL condition. The computation time is not less than 12 times the through-flow period (the period required by the mean flow to pass through the total domain once), and the results below are obtained by means of the time-weighted average of the last 6 periods. The classical γ-$Re_{\theta t}$ transition model is also activated for the SST and MST models.

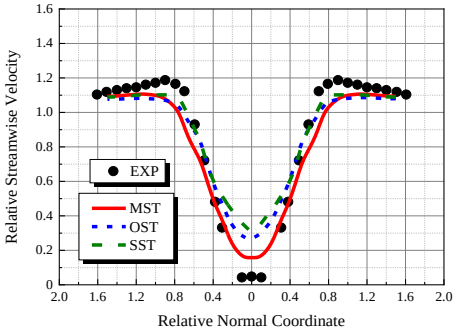

(a) Dimensionless streamwise velocity

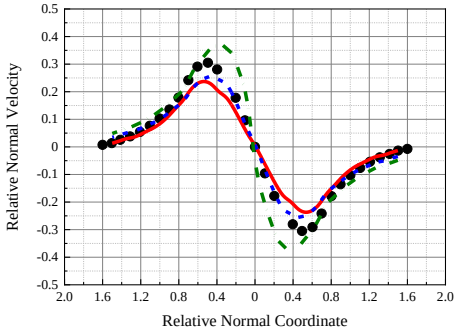

(b) Dimensionless normal velocity

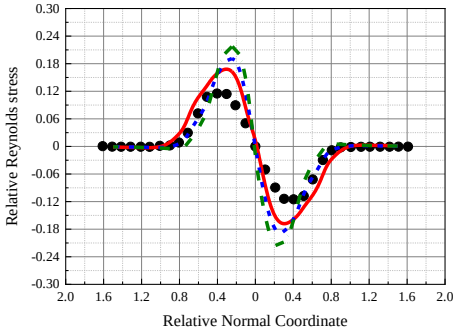

(c) Dimensionless Reynolds stress

Figure 11. Dimensionless mean values of velocity and Reynolds stress

Table 3. Comparisons of the vortex shedding frequency and flow separation position

	Vortex shedding frequency / (Hz)	Relative error	Flow separation position / (°)	Relative error
EXP	38.47	-	77	-
MST	38.33	0.36%	78.76	2.29%
OST	44.99	16.95%	83.11	7.94%
SST	49.98	29.92%	81.66	6.05%

The distributions of dimensionless mean streamwise velocity V_x/V_0, mean normal velocity V_y/V_0 and RMS Reynolds stress v_xv_y/V_0^2 on the measured line ($x=D$) are shown in Fig. 11. It is observed that the accuracy of MST model is better than the OST and SST models. In addition, the comparisons of the vortex shedding frequency and flow separation position are shown in Table 3.

The relative error of vortex shedding frequency obtained by the MST model is within 0.5%, while the values obtained by the OST and SST models are much higher. The relative error of flow separation position obtained by MST model is approximately 2%, which is the lowest and acceptable for engineering computations. Moreover, as shown in Fig. 12, the vortical structures are visualized by the isosurfaces of *Liutex* criterion. More detailed structures of vortex street are captured by the MST model.

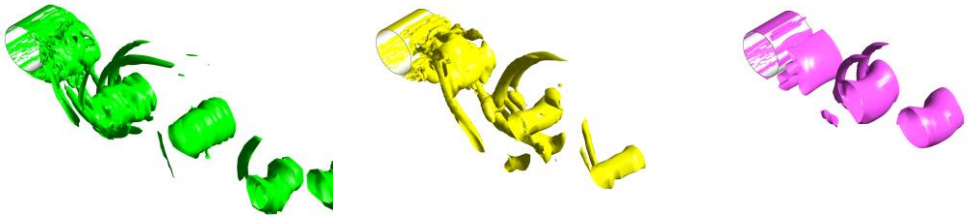

(a) MST (b) OST (c) SST

Figure 12. Vortex street visualized by *Liutex* isosurfaces (*Liutex*=300s^{-1})

3.4 Taylor-Couette flow

Taylor-Couette flow is one of the paradigmatic systems of the physics of fluids, which is characterized by the flow between two coaxial and independently rotating cylinders. The computation domain used for this flow case is shown in Fig. 13. The inner cylinder is rotating at a constant circumferential velocity, and the outer cylinder is at rest. The Reynolds number based on the inner radius R_1, outer radius R_2 and circumferential velocity of inner wall U_0 is 8000, and the Taylor number is 6.4×10^7.

High quality hexahedral grids consistent with literatures [45-46] are adopted to discretize the domain. The periodic conditions are employed in the axial direction, and the no-slip conditions are used for the two cylinder surfaces. The key parameter t_m of the OST model is set to 16s.

The distribution of RMS circumferential velocity is shown in Fig. 14. Again, the accuracy of MST model is significantly better than the OST and SST models, capturing more turbulent fluctuations.

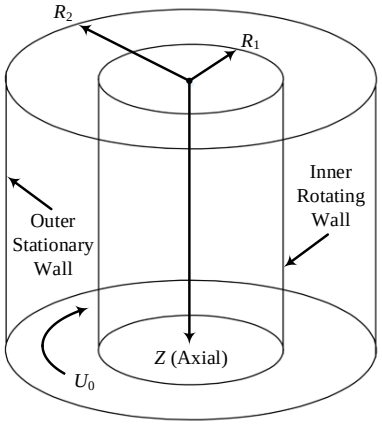

Figure 13. Computation domain of TC flow

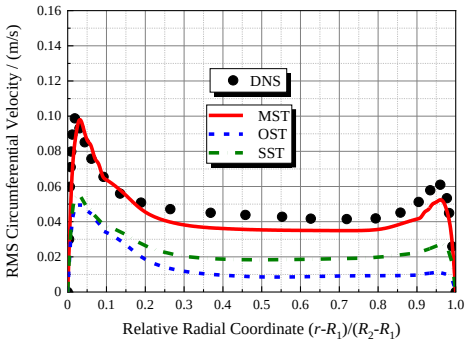

Figure 14. RMS circumferential velocity

3.5 Flow in a Centrifugal Pump Impeller

Turbulent flow in a centrifugal pump impeller is a typical flow case of hydraulic rotating machineries, which is strongly affected by the effects of rotation and curvature. The computation

domain adopted in this study is shown in Fig. 15, corresponding to the experiment [47-48]. The Reynolds number based on the impeller inlet diameter D_1 and the rated flowrate Q_0 is approximately 5.5×10^4. The circumferential velocity of impeller outlet U_2 based on the impeller outlet diameter D_2 and the rotating speed n is approximately 7.21m/s.

High quality hexahedral grids are adopted to discretize the domain, and the number of grids are approximately 1.60 million, which is determined on the basis of previous simulations of this flow case [48-49]. As for boundary conditions, the mass flowrate inlet condition with a low turbulence intensity is employed, while the pressure outlet condition and the no-slip wall condition are adopted.

Under the $1.0Q_0$ condition, blade-to-blade distributions of the mean relative circumferential velocity U_θ/U_2 (0.5-*spanwise* height), corresponding to the streamwise coordinate D/D_2 values of 0.5 and 0.75, are shown in Fig.16. Compared with the experimental data in two adjacent flow passages [47], the MST model gives a reasonably accurate prediction.

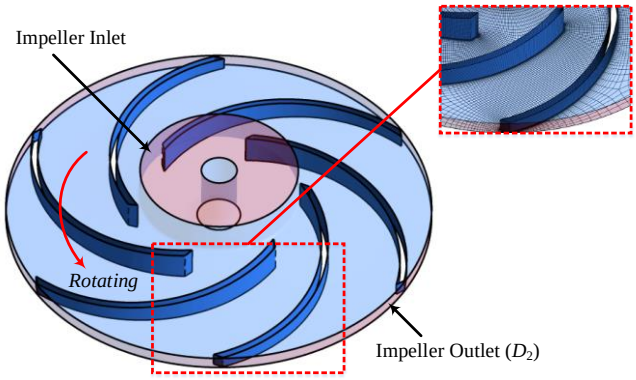

Figure 15. Computation domain of the centrifugal pump impeller

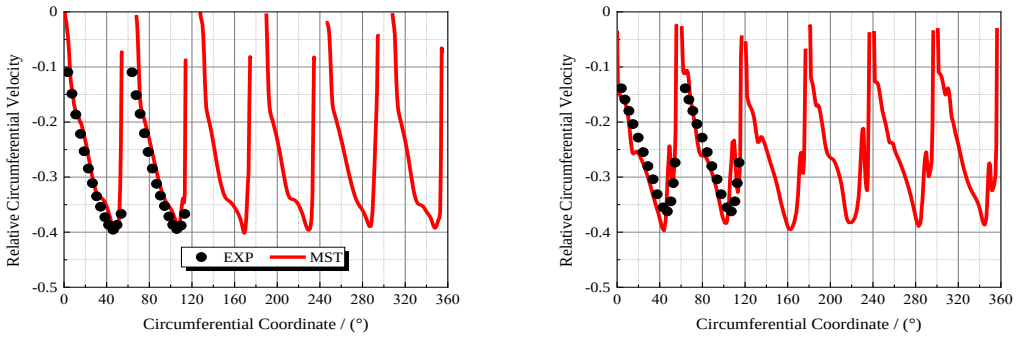

(a) D/D_2=0.50 (b) D/D_2=0.75

Figure 16. Mean relative circumferential velocity

Velocity contours in the impeller (0.5-*spanwise* height) are shown in Fig.17. Compared with the experimental results in two adjacent flow passages [47,50], typical features of velocity distribution are well predicted by the MST model. For example, the low speed areas caused by rotation instability near the blade pressure surfaces are captured, and the high speed areas near the blade suction surfaces and impeller outlet are resolved correctly. Moreover, under the $0.25Q_0$ condition, the important phenomenon, "*alternate stall*", is also well captured by the MST model, and the prediction results of stall cells are in agreement with those simulated by the LES method [48-49]. Again, it proves that the MST model is suitable for the computations of turbulent flows in the impeller, a core component of hydraulic rotating machineries.

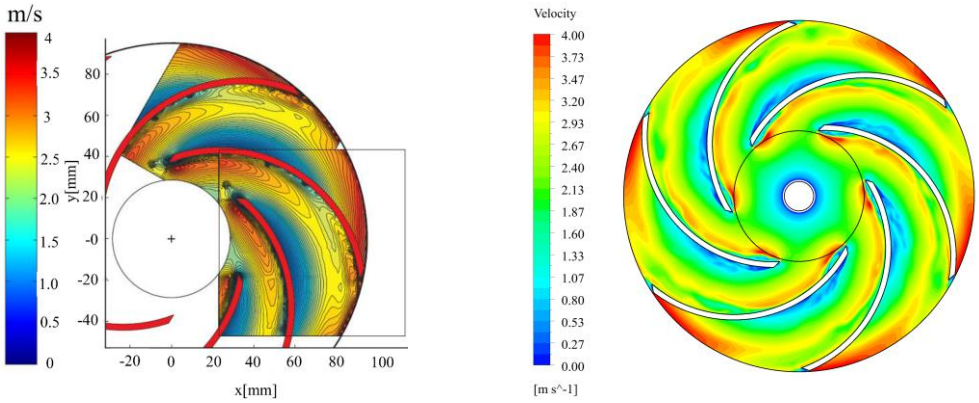

(a) EXP (b) MST

Figure 17. Velocity contours in the impeller ($1.0Q_0$ condition+0.5-*spanwise* height)

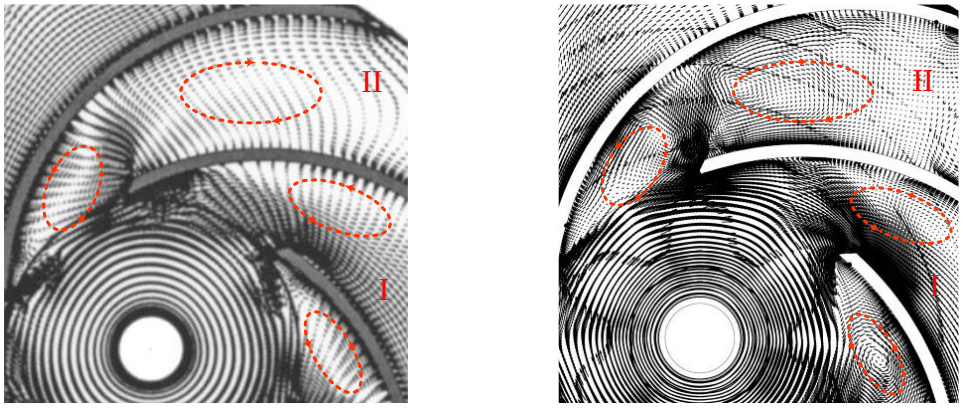

(a) LES (b) MST

Figure 18. Stall cells in the impeller ($0.25Q_0$ condition+0.5-*spanwise* height)

In summary, according to the test results of the above five classical flow cases, the MST model is more suitable for the numerical simulation of turbulent flows with rotation and curvature than the original STRUCT method, and it greatly improves engineering computations of turbulent flows in hydraulic rotating machineries.

4 Conclusions

In this study, a modified STRUCT model (*MST*) for the turbulent flows with rotation and curvature is proposed, and the conclusions are drawn as follows.

(1) The MST model, using the BSL k-ω model with the Spalart-Shur correction as the baseline, switches between URANS and LES-like modes by means of a new damping function D_f to adjust the turbulent viscosity μ_t. The new damping function D_f introduces the normalized helicity H_n to detect the energy backscatter phenomenon, and adopts a new adaptive timescale ratio R_t to avoid the arbitrariness of geometric averaging operation in the original STRUCT method.

(2) Comprehensive tests are carried out using five classical high Reynolds number flow cases (turbulent swirling flow through an abrupt axisymmetric expansion, flow around a hydrofoil, flow past a cylinder, Taylor-Couette flow and flow in a centrifugal pump impeller), and they confirm that the turbulent viscosity μ_t of the MST model is reasonably reduced in the massively separated regions, and the LES-like mode is activated, which allows more turbulent fluctuations and vortical structures to be captured on the same URANS grids.

(3) The MST model improves the prediction accuracy of turbulent flow fields with rotation and

curvature, while inherits the advantages of the original STRUCT method (high efficiency and robustness). It provides a good foundation for efficient engineering computations of turbulent flows in hydraulic rotating machineries.

Acknowledgments

The authors would like to acknowledge the financial support from the National Natural Science Foundation of China (No. 51836010, 51779258, 51839001), National Key Research and Development Program (No. 2018YFB0606103) and Beijing Nature Science Foundation (No. 3182018).

References

[1] Pinto R N, Afzal A, D'Souza L V, Ansari Z, Samee A D M. Computational fluid dynamics in turbomachinery: A review of state of the art. Archives of Computational Methods in Engineering 2017; 24(3): 467-479.

[2] Wang S Y, Ingham D B, Ma L, Pourkashanian M, Tao Z. Turbulence modeling of deep dynamic stall at relatively low Reynolds number. Journal of Fluids and Structures 2012; 33: 191-209.

[3] Yang Z Y. Large-eddy simulation: Past, present and the future. Chinese Journal of Aeronautics 2015; 28(1): 11-24.

[4] Gourdain N, Sicot F, Duchaine F, Gicquel L. Large eddy simulation of flows in industrial compressors: A path from 2015 to 2035. Philosophical Transactions of The Royal Society A-Mathematical Physical and Engineering Sciences 2014; 372(2022). 20130323.

[5] Fröhlich J, Terzi D V. Hybrid LES/RANS methods for the simulation of turbulent flows. Progress in Aerospace Sciences 2008; 44(5): 349-377.

[6] Chaouat B. The state of the art of hybrid RANS/LES modeling for the simulation of turbulent flows. Flow, Turbulence and Combustion 2017; 99(2): 279-327.

[7] Spalart P R, Jou W H, Strelets M, Allmaras S R. Comments on the feasibility of LES for wings, and on a hybrid RANS/LES approach. In: Advances in DNS/LES. Greyden Press, Columbus, OH, USA; 1997.

[8] Spalart P R, Deck S, Shur M L, Squires K D, Strelets M K, Travin A. A new version of detached-eddy simulation, resistant to ambiguous grid densities. Theoretical and Computational Fluid Dynamics 2006; 20(3): 181-195.

[9] Shur M L, Spalart P R, Strelets M K, Travin A. A hybrid RANS-LES approach with delayed-DES and wall-modelled LES capabilities. International Journal of Heat and Fluid Flow 2008; 29(6): 1638-1649.

[10] Speziale C. Turbulence modeling for time-dependent RANS and VLES: A review. AIAA Journal 1998; 36(2): 173-184.

[11] Hsieh K J, Lien F S, Yee E. Towards a unified turbulence simulation approach for wall-bounded flows. Flow Turbulence & Combustion 2010; 84(2): 193-218.

[12] Han X, Krajnović S. Validation of a novel very large eddy simulation method for simulation of turbulent separated flow. International Journal for Numerical Methods in Fluids 2013; 73(5): 436-461.

[13] Girimaji S S. Partially-averaged Navier-Stokes model for turbulence: A Reynolds-averaged Navier-Stokes to direct numerical simulation bridging method. Journal of Applied Mechanics 2006; 73(3): 413-421.

[14] Foroutan H, Yavuzkurt S. A partially-averaged Navier-Stokes model for the simulation of turbulent swirling flow with vortex breakdown. International Journal of Heat and Fluid Flow 2014; 50: 402-416.
[15] Ma J M, Peng S H, Davidson H, Wang F J. A low Reynolds number variant of partially-averaged Navier-Stokes model for turbulence. International Journal of Heat and Fluid Flow 2011; 32: 652-669.
[16] Menter F R, Kuntz M, Bender R. A scale-adaptive simulation model for turbulent flow predictions. In: 41st Aerospace Sciences Meeting and Exhibit, Reno, Nevada, USA; 2003.
[17] Egorov Y, Menter F R. Development and application of SST-SAS turbulence model in the DESIDER Project. Advances in Hybrid RANS-LES Modelling 2008; NNFM 97: 261-270.
[18] Mehdizadeh A, Foroutan H, Vijayakumar G, Sadiki A. A new formulation of scale-adaptive simulation approach to predict complex wall-bounded shear flows. Journal of Turbulence 2014; 15(10): 629-649.
[19] Johansen S T, Wu J Y, Shyy W. Filter-based unsteady RANS computations. International Journal of Heat and Fluid Flow 2004; 25(1): 10-21.
[20] Liu H L, Wang Y, Liu D X, Yuan S Q, Wang J. Assessment of a turbulence model for numerical predictions of sheet-cavitating flows in centrifugal pumps. Journal of Mechanical Science and Technology 2013; 27(9): 2743-2750.
[21] Wilcox D C. Turbulence Modeling for CFD. California, USA: DCW Industries; 2006.
[22] Baglietto E, Lenci G, Concu D. STRUCT: A second-generation URANS approach for effective design of advanced systems. In: ASME Fluids Engineering Division Summer Meeting, Hawaii, USA; 2017.
[23] Lenci G. A methodology based on local resolution of turbulent structures for effective modeling of unsteady flows. Ph.D. dissertation, Massachusetts Institute of Technology, USA; 2016.
[24] Feng J Y, Frahi T, Baglietto E. STRUCTure-based URANS simulations of thermal mixing in T-junctions. Nuclear Engineering and Design 2018; 340: 275-299.
[25] Liu Y W, Lu L P, Fang L, Gao F. Modification of Spalart-Allmaras model with consideration of turbulence energy backscatter using velocity helicity. Physics Letters A 2011; 375(24): 2377-2381.
[26] Perot J B, Gadebusch J. A self-adapting turbulence model for flow simulation at any mesh resolution. Physics of Fluids 2007; 19(11). 115105.
[27] Menter F R. Two-equation eddy-viscosity turbulence models for engineering applications. AIAA Journal 1994; 32(8): 1598-1605.
[28] Spalart P R, Shur M. On the sensitization of turbulence models to rotation and curvature. Aerospace Science and Technology 1997; 1(5): 297-302.
[29] Scheeler M W, Rees W M V, Kedia H, Kleckner D, Irvine W T M. Complete measurement of helicity and its dynamics in vortex tubes. Science 2017; 357(6350): 487-491.
[30] Moffatt K H. Helicity-invariant even in a viscous fluid. Science 2017; 357(6350): 448-449.
[31] Belian A, Chkhetiani O, Golbraikh E, Moiseev S. Helical turbulence: Turbulent viscosity and instability of the second moments. Physica A 1998; 258: 55-68.
[32] Yu C P, Hong R K, Xiao Z L, Chen S Y. Subgrid-scale eddy viscosity model for helical turbulence. Physics of Fluids 2013; 25(9). 095101.
[33] Dellenback P A, Metzger D E, Neitzel G P. Measurements in turbulent swirling flow through

an abrupt axisymmetric expansion. AIAA Journal 1988; 26(6): 669-681.
[34] Gyllenram W, Nilsson H. Design and validation of a scale-adaptive filtering technique for LRN turbulence modeling of unsteady flow. Journal of Fluids Engineering 2008; 130(5). 051401.
[35] Paik J, Sotiropoulos F. Numerical simulation of strongly swirling turbulent flows through an abrupt expansion. International Journal of Heat and Fluid Flow 2010; 31(3): 390-400.
[36] Liu C Q, Gao Y S, Dong X R, Wang Y Q, Liu J M, Zhang Y N, Cai X S, Gui N. Third generation of vortex identification methods: Omega and Liutex/Rortex based systems. Journal of Hydrodynamics 2019; 31(2): 205-223.
[37] Ausoni P. Turbulent vortex shedding from a blunt trailing edge hydrofoil. Ph.D. dissertation, Swiss Federal Institute of Technology Lausanne, Switzerland; 2009.
[38] Ausoni P, Zobeiri A, Avellan F, Farhat M. The effects of a tripped turbulent boundary layer on vortex shedding from a blunt trailing edge hydrofoil. Journal of Fluids Engineering 2012; 134(5). 051207.
[39] Li Y J, Chen J, Yao Z F, Liu Z Q, Yang W. Numerical investigation of flow around blunt trailing edge hydrofoil using transition SST model. Journal of Hydraulic Engineering 2017; 48(8): 993-1001.
[40] Zeng Y S, Yao Z F, Zhou P J, Wang F J, Hong Y P. Numerical investigation into the effect of the trailing edge shape on added mass and hydrodynamic damping for a hydrofoil. Journal of Fluids and Structures 2019; 88: 167-184.
[41] Cantwell B, Coles D. An experimental study of entrainment and transport in the turbulent near wake of a circular cylinder. Journal of Fluid Mechanics 1983; 136: 321-374.
[42] Breuer M. A challenging test case for large eddy simulation: High Reynolds number circular cylinder flow. International Journal of Heat and Fluid Flow 2000; 21: 648-654.
[43] Qu L X, Norberg C, Davidson L, Peng S H, Wang F J. Quantitative numerical analysis of flow past a circular cylinder at Reynolds number between 50 and 200. Journal of Fluids and Structures 2013; 39: 347-370.
[44] Karabelas S J. Large eddy simulation of high-Reynolds number flow past a rotating cylinder. International Journal of Heat and Fluid Flow 2010; 31(4): 518-527.
[45] Dong S. Direct numerical simulation of turbulent Taylor-Couette flow. Journal of Fluid Mechanics 2007; 587: 373-393.
[46] Grossmann S, Lohse D, Sun C. High-Reynolds number Taylor-Couette turbulence. Annual Review of Fluid Mechanics 2016; 48(1): 53-80.
[47] Byskov R K, Jacobsen C B, Pedersen N. Flow in a centrifugal pump impeller at design and off-design donditions-Part I: particle image velocimetry (PIV) and laser doppler velocimetry (LDV) measurements. Journal of Fluids Engineering 2003; 125(1): 61-72.
[48] Byskov R K, Jacobsen C B, Pedersen N. Flow in a centrifugal pump impeller at design and off-design donditions-Part II: large eddy simulations. Journal of Fluids Engineering 2003; 125(1): 73-83.
[49] Huang X B, Liu Z Q, Yang W. Comparative study of SGS models for simulating the flow in a centrifugal-pump impeller using single passage. Engineering Computations 2015; 32(7): 2120-2135.
[50] Yao Z F, Yang Z J, Wang F J. Evaluation of near-wall solution approaches for large-eddy simulations of flow in a centrifugal pump impeller. Engineering Applications of Computational Fluid Mechanics 2016; 10(1): 454-467.